



**HAL**  
open science

## Molecular dynamics simulation of the effect of pH on the adsorption of rhodamine laser dyes on TiO<sub>2</sub> hydroxylated surfaces

Said Hamad, Juan Ramon Sanchez Valencia, Angel Barranco, Jose Antonio Mejias, Agustin R González-Elipe

► **To cite this version:**

Said Hamad, Juan Ramon Sanchez Valencia, Angel Barranco, Jose Antonio Mejias, Agustin R González-Elipe. Molecular dynamics simulation of the effect of pH on the adsorption of rhodamine laser dyes on TiO<sub>2</sub> hydroxylated surfaces. *Molecular Simulation*, 2009, 35 (12-13), pp.1140-1151. 10.1080/08927020903108083 . hal-00530458

**HAL Id: hal-00530458**

**<https://hal.science/hal-00530458>**

Submitted on 29 Oct 2010

**HAL** is a multi-disciplinary open access archive for the deposit and dissemination of scientific research documents, whether they are published or not. The documents may come from teaching and research institutions in France or abroad, or from public or private research centers.

L'archive ouverte pluridisciplinaire **HAL**, est destinée au dépôt et à la diffusion de documents scientifiques de niveau recherche, publiés ou non, émanant des établissements d'enseignement et de recherche français ou étrangers, des laboratoires publics ou privés.

**Molecular dynamics simulation of the effect of pH on the adsorption of rhodamine laser dyes on TiO<sub>2</sub> hydroxylated surfaces**

Journal:	<i>Molecular Simulation/Journal of Experimental Nanoscience</i>
Manuscript ID:	GMOS-2009-0023.R1
Journal:	Molecular Simulation
Date Submitted by the Author:	18-Apr-2009
Complete List of Authors:	Hamad, Said; Institute of Materials Science of Seville, CSIC - University of Seville; University Pablo de Olavide, Department for physical, chemical and natural systems Sanchez Valencia, Juan Ramon; Institute of Materials Science of Seville, CSIC - University of Seville Barranco, Angel; Institute of Materials Science of Seville, CSIC - University of Seville Mejias, Jose Antonio; University Pablo de Olavide, Department for physical, chemical and natural systems González-Elipe, Agustin; Institute of Materials Science of Seville, CSIC - University of Seville
Keywords:	Rhodamine, adsorption, TiO <sub>2</sub> , anatase, simulation

SCHOLARONE™  
Manuscripts

# Molecular dynamics simulation of the effect of pH on the adsorption of rhodamine laser dyes on TiO<sub>2</sub> hydroxylated surfaces

Said Hamad<sup>1,2\*</sup>, Juan Ramon Sanchez-Valencia<sup>1</sup>, Angel Barranco<sup>1</sup>, Jose Antonio Mejias<sup>2</sup> and Agustin

R. Gonzalez-Elipe<sup>1</sup>

- 1) Instituto de Ciencia de Materiales de Sevilla, CSIC-Universidad de Sevilla, Calle Américo Vespucio, nº 49, 41092, Seville, Spain.
- 2) University Pablo de Olavide, Department of Physical, Chemical and Natural Systems, Carretera de Utrera, km 1, Seville, Spain.

We have carried out a study of the adsorption, on the (101) surface of anatase TiO<sub>2</sub>, of two industrially relevant rhodamines molecules (rhodamine 6G and rhodamine 800) employing Molecular Dynamics. These theoretical studies have shown that Rhodamine 6G must adsorb on surfaces under basic conditions. Moreover, the adsorption of this molecule shows a strong dependence upon the pH of the system, i.e. under basic conditions the adsorption energy is quite high, under neutral conditions the adsorption energy is lower, and under acidic conditions an even lower adsorption energy indicates that there must be very little adsorption under such conditions.

By contrast, for rhodamine 800 there is little dependence of the adsorption energy upon the pH, suggesting that the amount of adsorption of this molecules is little affected by this parameter.

These theoretical results are in qualitative agreement with ~~the~~ experimental results consisting of the incorporation of these dye molecules into porous thin films.

Deleted:

Deleted: quite

Deleted: smaller

Deleted: being

Deleted: expected

1  
2  
3  
4  
5  
6  
7  
8  
9  
10  
11  
12  
13  
14  
15  
16  
17  
18  
19  
20  
21  
22  
23  
24  
25  
26  
27  
28  
29  
30  
31  
32  
33  
34  
35  
36  
37  
38  
39  
40  
41  
42  
43  
44  
45  
46  
47  
48  
49  
50  
51  
52  
53  
54  
55  
56  
57  
58  
59  
60

*Keywords:* Rhodamine, adsorption, TiO<sub>2</sub>, anatase, (101) surface, Molecular Dynamics, PZC.

For Peer Review Only

## 1. Introduction

Rhodamines are biocompatible, photostable and luminescent dye molecules, widely used for a large variety of applications including laser, probe molecule of surface states, solar cells, or surface coatings<sup>1-4</sup>. For the majority of these uses, the dye molecule has to be incorporated into a solid, a feature that has fostered both the development of new synthesis and processing methods of the final materials and the study of their optical and fluorescent behaviours. Thus, for example, it has been shown that rhodamine-G molecules can be easily incorporated within the interlayer space of silicates and other layered materials<sup>5-9</sup>. The incorporation of these molecules into sol-gel silica, mesoporous TiO<sub>2</sub> thin films or into polymeric matrices has been also intended for the fabrication of optical components and devices<sup>10-13</sup>.

Recently, we have shown that R6G and R800 dye molecules can be incorporated within transparent and porous films of TiO<sub>2</sub> or Ta<sub>2</sub>O<sub>5</sub> prepared by glancing angle evaporation just by immersing the films into an aqueous solution of the two dye molecules in cationic form<sup>14</sup>. The incorporation of the dye molecules into the film was driven by the pH of their solution and, in the case of the R6G, explained by using the classical concepts of the point of zero charge (PZC) developed in the 1960's to account for the adsorption of ions on the surface of colloidal oxides<sup>15</sup>. The results represents a clear evidence for the importance of the interaction of the hydroxylated porous oxide surfaces with the cationic dye molecules during the absorption processes. In particular, we found that the R6G only starts to become incorporated within the pores of the films when the pH of the solution was approaching or was higher than the PZC of TiO<sub>2</sub> (i.e., around 5.5 (refs. 14 and 15)). The simplicity of the experimental method used for the preparation of these composite thin films has motivated the present theoretical work, where we account for the different effect of the pH and on the adsorption of R6G and R800 on the surface of TiO<sub>2</sub>. For this purpose we present here a theoretical study by using Molecular Dynamics techniques to obtain

information about the adsorption of these two dye molecules. The results obtained can be of relevance for the study of other types of composite materials consisting of dye molecules adsorbed on the surface of TiO<sub>2</sub>. A classical example in this respect is that of the Grätzel solar cells<sup>16,17</sup>. In this context, previous theoretical studies in the literature have dealt with the adsorption of Ru(II)-polypyridyl dyes on the surface of an ideal TiO<sub>2</sub> surface<sup>18</sup>. However, to our knowledge, no theoretical studies have been carried out to investigate the interaction of these or similar dye molecules with a hydroxylated surface of this oxide, taking into account the effect of pH on their adsorption. For the present study, we have used four different types of surfaces, on which to model the adsorption of the rhodamine molecules. The chosen models of surfaces provide a description of the adsorption on non-hydroxylated surfaces, as well as on surfaces under basic, neutral and acidic conditions.

## 2. Computational details

The first step in any Molecular Dynamics (MD) simulation is the compilation of an adequate set of interatomic potentials to model the system. Our experimental observations require the use of computational features which are somehow more complicated than those of usual MD simulations, since we need to model the influence of hydroxylation and pH. TiO<sub>2</sub> surfaces are usually modelled as clean, non-hydrated, non-hydroxylated surfaces, although there are some exceptions in literature<sup>23-27</sup>. The initial set of parameters used to model the TiO<sub>2</sub> (101) anatase surface were taken from the modification that Predota et al.<sup>23,28</sup> made of the Matsui and Akaogi potentials<sup>29</sup> to study (110) rutile hydroxylated surfaces. The parameters presented by Predota et al.<sup>23,28</sup> were not optimised to model the hydroxylated (101) anatase surface, and when they were used to minimise the surface, we observed the rupture of O-H bonds upon minimisation.

### Deleted: 2. Experimental details and materials

Composite R6G/TiO<sub>2</sub> and R800/TiO<sub>2</sub> thin films were prepared by using porous TiO<sub>2</sub> thin films as host materials. For this purpose, transparent and amorphous TiO<sub>2</sub> were prepared by Glancing Angle Physical Vapor Deposition (GAPVD) at room temperature on quartz and silicon substrates. Evaporation was carried out in an electron bombardment evaporator by using TiO<sub>2</sub> pellets as target material. Stoichiometric thin films of TiO<sub>2</sub> were obtained by performing the evaporation in 10<sup>-4</sup> torrs of O<sub>2</sub>. The evaporation was carried out by placing the substrates at a glancing angle of 70° with respect to the evaporator source. This geometry produces films with a tilted columnar microstructure with a high porosity<sup>19,21</sup>. The films with a thickness around 400 nm were prepared by this method. In the present case the porosity of the films was estimated to be 35% of the total volume of the films, with a 70% of pores consisting of mesopores. A full account of the characteristics of these films can be found in a previous publication<sup>14</sup>. The microstructure of the TiO<sub>2</sub> thin films deposited on a silicon wafer was examined by Field Emission Scanning Electron Microscopy (FESEM) in a Hitachi S5200 microscope. Cross sectional views were obtained by cleaving the silicon substrates. UV-visible absorption spectra in transmission mode were recorded with a Perkin-Elmer Lambda 12 spectrometer for the thin films deposited on quartz plates. Although the absorbance is the typical magnitude used for presenting UV-vis absorption spectra of dyes in liquid solutions, we present here some spectra as the percentage of transmitted light. We have made this choice because this is the usual way of presenting these data when using optical thin films<sup>22</sup>. A chloride salt of R6G and R800 dye molecules was used for the experiments. The salts were supplied by ALDRICH and used without further purification. In solution, the cationic R6G or R800 bear a positive charge, a feature that is essential for the incorporation of the dye into the TiO<sub>2</sub> thin films. A 10<sup>-4</sup> M solutions of the dyes in water at controlled values of pH were used for the infiltration experiments. The pH of the solution was controlled between 1.9 and 6.6 by adding giving amounts of HCl or NaOH. The TiO<sub>2</sub> films were immersed in one of these solutions and maintained there for 10 min. The samples were then removed from the solution and washed with water at the same pH than that of the dye solutions. In general, the intensity of the colour of the films changed with the pH of the solution, a feature that suggests the dependence between this parameter and the ability to incorporate the dye molecules into the films. Figure 1 shows a series of UV-vis transmission spectra recorded for ... [1]

Therefore, some changes were introduced into the interatomic potentials to allow us to study of the hydroxylated (101) anatase surface. In order to have a reference to test the results of the changes of the interatomic potentials parameters, we carried out the optimisation of a hydroxylated (101) anatase surface with the Density Functional Theory (DFT), using the plane-wave-pseudopotential approach within the projector augmented wave method (PAW)<sup>30</sup>, together with the Generalized Gradient Approximation (GGA) exchange correlation functional proposed by Perdew et al.<sup>31</sup>, as implemented in the Vienna Ab-initio Simulation Package (VASP) 4.6 code<sup>32-34</sup>. A plane-wave cutoff energy of 400 eV was used. The Ti (3s, 3p, 3d, 4s), O (2s, 2p) and H (1s) electrons were treated as valence states, while the remaining electrons were kept frozen as core states. The Brillouin-zone integrations were performed using Monkhorst-Pack grids<sup>35</sup>. The slab approximation was used to model the surface, with a TiO<sub>2</sub> slab thickness of 20Å, and a vacuum slab of 10Å. The cell dimensions are 5.44Å×3.78Å×30.0Å. The calculations were carried out by using a (7×7×1) mesh, with which convergence in energy was achieved.

In order to get a good agreement with the geometries obtained with the DFT calculations, we made some modifications in the interatomic potentials. Since one of the requirements was the modelling of the O-H bonds at the surface (such as bonds 2-3 and 4-5 in Figure 1), we introduced a harmonic force between the O and H atoms of the surface hydroxyl groups of the form  $E = 1/2 \cdot k_1 \cdot (r-r_0)^2$ . The values of the parameters were:  $k_1=500.4 \text{ kcal mol}^{-1}/\text{Å}^2$  and  $r_0=0.95\text{Å}$ . Another important parameter in the description of the surface is the harmonic force that predicts a correct value of the Ti-O-H angles such as the angles 1-2-3 and 1-4-5 in Figure 1. This force is of the form  $E = 1/2 \cdot k_2 \cdot (\theta-\theta_0)^2$ , where  $\theta$  is the angle between the three atoms,  $\theta_0$  is the equilibrium value of this angle, around which  $\theta$  oscillates and  $k_2$  is the constant of the harmonic force that induces these oscillations. For O-H groups connected to terminal Ti atoms we did not change the parameters, but for O-H groups where the O involved is a bridging O (such as atom 4 in Figure 1), the new

Deleted: .

Deleted:

parameters are  $k_2=14.136 \text{ kcal mol}^{-1} \text{ rad}^{-2}$  and  $\theta_0=120^\circ$ . The geometry of the hydroxylated (101) anatase surface obtained with this new set of interatomic potentials is in reasonable good agreement with that obtained with DFT calculations, as shown in Table 2. The larger disagreement, as expected, is found for the distance between atoms 5 and 11, since they interact by a weak hydrogen bond, a situation which is difficult to model accurately using interatomic potentials.

To model the rhodamine molecules we have employed the DREIDING force field<sup>36</sup>, which was developed to predict structures and dynamics of organic, biological and main-group inorganic molecules. The van der Waals parameters of the DREIDING force field are taken from the Williams potentials<sup>37,38</sup>, including some modifications. The electrostatic charges were calculated with *ab initio* calculations, by fitting the electrostatic potential at points selected according to the Merz-Singh-Kollman scheme<sup>39,40</sup>, as implemented in the program Gaussian03<sup>41</sup>. The Becke three parameter hybrid functional<sup>42</sup> (B3LYP) was used to fit the atomic charges, together with a 6-31+G\* basis set. SI Table 1 and SI Table 2 show the atomic charges as well as the force type assignments. This level of theory has been previously used to study other dyes<sup>43</sup>. The DREIDING force field predicts an equilibrium angle of  $\sim 40^\circ$  between the xantheno and phenyl moieties that form the rhodamine 6G molecule, whereas *ab initio* calculations predict that the planes of the two moieties lie perpendicular to each other. In order to predict correctly this angle of  $90^\circ$ , we included an additional torsional term in the force field. In DREIDING, the torsion interaction for two bonds (those between atoms IJ and KL) connected via a common bond JK takes the form,

$$E_{IJKL} = \frac{1}{2} V_{JK} \left\{ 1 - \cos \left[ n_{JK} (\varphi - \varphi_{JK}^0) \right] \right\},$$

where  $\varphi$  is the dihedral angle (angle between the IJK and JKL planes),  $n_{JK}$  is the periodicity (an integer),  $V_{JK}$  is the barrier for rotation (always positive), and  $\varphi_{JK}^0$  is the equilibrium angle. We did

Deleted:

1 not carried out a parameter fitting in order to obtain the value of the parameters needed to model  
2 correctly the angle between the two moieties. Instead, we introduced an additional term, taking the  
3 same parameters that describe the torsion of a dihedral resonance bond (bond order = 1.5)  
4 involving two resonant atoms, namely  $V_{JK} = 25$  kcal/mol,  $n_{JK} = 2$ , and changing the equilibrium  
5 angle from  $\varphi_{JK}^0 = 180^\circ$  to  $\varphi_{JK}^0 = 90^\circ$ . This torsional force is only included to model the interaction  
6 between atoms C9 and C14 in Figure 2a. We checked the validity of this term by comparing the  
7 variation of the energy with respect to the rotation angle, **this latter** obtained with the interatomic  
8 potentials discussed and two ab initio methods: B3LYP/6-31+G\* and MP2/6-31++G\*\*. The  
9 results are shown in Figure 3. In the most critical region, between  $90^\circ$  and  $110^\circ$ , the three methods  
10 predict essentially the same dependency with respect to the rotation. For angles higher than  $110^\circ$   
11 the less accurate methods (interatomic potentials and B3LYP/6-31+G\*) predict a different change  
12 in energy than MP2/6-31++G\*\*, although at  $120^\circ$  the energy difference is still less than 3  
13 kcal/mol. We can therefore consider that the DREIDING force field, with this additional term,  
14 predicts correctly the behaviour of rhodamine 6G. In the case of rhodamine 800 there is no need to  
15 include any additional terms, since the DREIDING force field describes it correctly. The van der  
16 Waals interaction between the rhodamine molecules and the surface are taken from the  
17 DREIDING force field. The existence of parameters to describe the interaction between the  
18 molecules and the  $\text{TiO}_2$  surface (which is not the case for other force fields such as AMBER or  
19 CHARMM) is the main reason why the DREIDING force field is used.

20  
21  
22  
23  
24  
25  
26  
27  
28  
29  
30  
31  
32  
33  
34  
35  
36  
37  
38  
39  
40 All interatomic potentials based energy minimisations and Molecular Dynamics  
41 simulations have been performed with the GULP code<sup>44</sup>, at the high performance computing  
42 facilities of CSIC in Madrid. The timestep for the integration of the equations of motion is 1fs.  
43 The systems are modelled in the canonical (NVT) ensemble, employing the Hoover thermostat,  
44 with a friction constant for the temperature bath of 0.1, to maintain the temperature around  $298^\circ\text{C}$ .

1  
2 The systems are equilibrated for 50 ps, followed by 100 ps of production. Since the number of  
3  
4 degrees of freedom associated with the motion of the rhodamine molecules is relatively small,  
5  
6 there is no need to perform very long simulations to sample the most relevant region of the phase  
7  
8 space.

9  
10 The *ab initio* calculations (using Gaussian03 and VASP) have been carried out in the Finis  
11  
12 Terrae supercomputer, in Santiago de Compostela, Spain.

Formatted: English U.K.

Deleted: 4

Deleted: ¶

### 3. Materials, Theoretical Results and Discussion

#### 3.1. Experimental details and materials.

23  
24 Composite R6G/TiO<sub>2</sub> and R800/TiO<sub>2</sub> thin films were prepared by using porous TiO<sub>2</sub> thin  
25 films as host materials. For this purpose, transparent and amorphous TiO<sub>2</sub> were prepared by  
26 Glancing Angle Physical Vapor Deposition (GAPVD) at room temperature on quartz and silicon  
27 substrates. Evaporation was carried out in an electron bombardment evaporator by using TiO<sub>2</sub>  
28 pellets as target material. Stoichiometric thin films of TiO<sub>2</sub> were obtained by performing the  
29 evaporation in 10<sup>-4</sup> torrs of O<sub>2</sub>. The evaporation was carried out by placing the substrates at a  
30 glancing angle of 70° with respect to the evaporator source. This geometry produces films with a  
31 tilted columnar microstructure and a high porosity<sup>19-21</sup>. Thin films with a thickness around 400 nm  
32 were prepared by this method. In the present case the porosity of the films was estimated to be  
33 35% of the total volume of the films, with a 70% of pores consisting of mesopores. A full account  
34 of the characteristics of these films can be found in a previous publication<sup>14</sup>.

1  
2  
3  
4  
5  
6  
7  
8  
9  
10  
11  
12  
13  
14  
15  
16  
17  
18  
19  
20  
21  
22  
23  
24  
25  
26  
27  
28  
29  
30  
31  
32  
33  
34  
35  
36  
37  
38  
39  
40  
41  
42  
43  
44  
45  
46  
47  
48  
49  
50  
51  
52  
53  
54  
55  
56  
57  
58  
59  
60

The microstructure of the TiO<sub>2</sub> thin films deposited on a silicon wafer was examined by Field Emission Scanning Electron Microscopy (FESEM) in a Hitachi S5200 microscope. Cross sectional views were obtained by cleaving the silicon substrates.

UV-visible absorption spectra in transmission mode were recorded with a Perkin-Elmer Lambda 12 spectrometer for the thin films deposited on quartz plates. Although the absorbance is the typical magnitude used for presenting UV-vis absorption spectra of dyes in liquid solutions, we present here some spectra as the percentage of transmitted light. We have made this choice because this is the usual way of presenting these data when using optical thin films<sup>22</sup>.

A chloride salt of R6G and R800 dye molecules was used for the experiments. The salts were supplied by ALDRICH and used without further purification. In solution, the cationic R6G or R800 bear a positive charge, a feature that is essential for the incorporation of the dye into the TiO<sub>2</sub> thin films.

A 10<sup>-4</sup> M solutions of the dyes in water at controlled values of pH were used for the infiltration experiments. The pH of the solution was controlled between 1.9 and 6.6 by adding given amounts of HCl or NaOH. The TiO<sub>2</sub> films were immersed in one of these solutions and maintained there for 10 min. The samples were then removed from the solution and washed with water at the same pH than that of the dye solutions. In general, the intensity of the colour of the films changed with the pH of the solution, a feature that suggests the dependence between this parameter and the ability to incorporate the dye molecules into the films.

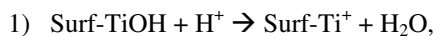
shows a series of UV-vis transmission spectra recorded for TiO<sub>2</sub> thin films containing different concentrations of R6G and R800, as indicated in Table 1. The spectra are characterized by the presence of a series of bands typical of the R6G dye molecules (i.e., bands centred at ~520 nm) and R800 (i.e., bands centred at ~650 nm)<sup>14</sup> superimposed on the typical oscillations due to

1 interference phenomena between a substrate and a transparent layer of different refraction index<sup>14</sup>.  
2  
3 For the purposes of the present work, the most important result is the dependence of the intensity  
4 of the features attributed to the two dye molecules and the pH of the solution used for the  
5 preparation of the films. Thus, it is observed that the intensity of the R6G features are strongly  
6 dependent on the pH, increasing with this parameter. By contrast, R800 is little or no sensitive to  
7 this parameter and the intensity of its spectral features remains almost invariable for all the pHs.  
8 This different behaviour suggests that these two molecular cations interact differently with the  
9 surface of TiO<sub>2</sub> and that, particularly for the R800, the state of charge on the TiO<sub>2</sub> does not affect  
10 significantly the adsorption of this molecule.  
11  
12  
13  
14  
15  
16  
17  
18  
19  
20  
21  
22  
23

### 24 3.2. Theoretical results and discussion.

25  
26 Once a suitable set of interatomic potentials is obtained, we created the unit cells that  
27 model the systems of interest. The simplest cell to study the adsorption of rhodamines is a bare  
28 surface formed by a slab of TiO<sub>2</sub> in vacuum. We generated a 17 Å slab exposing the (101) surface  
29 of anatase TiO<sub>2</sub>, with a (6 a<sub>x</sub> x 8 a<sub>y</sub>) periodic replication of the elementary experimental cell of  
30 dimensions a<sub>x</sub>=5.44 Å and a<sub>y</sub>=3.776 Å. The simulation cell contains 10 Ti atoms and 20 O atoms,  
31 giving a total of 480 Ti atoms and 960 O atoms. The dimensions of the unit cell are 32.66 Å x 30.2  
32 Å x 50 Å, and the angle between a<sub>x</sub> and a<sub>y</sub> is 110.30°. There is a vacuum gap of 33 Å between the  
33 slabs. The charges on the Ti and O atoms are 2.196e and -1.098e respectively. Since we are  
34 interested in studying the effect of pH on the adsorption energy (E<sub>ad</sub>) of rhodamines, we also  
35 generated three unit cells to model different values of pH: 1) hydroxylated surface under neutral  
36 conditions, 2) hydroxylated surface under acidic conditions and 3) hydroxylated surface under  
37 basic conditions. Surface 1 is created by adding an H atom to each bridging O atom and a hydroxyl  
38  
39  
40  
41  
42  
43  
44  
45  
46  
47  
48  
49  
50  
51  
52  
53  
54  
55  
56  
57  
58  
59  
60

1 to each Ti atom, as shown in Figure 1. The charge of the O atoms in the hydroxyl groups is -  
2  
3 0.848e and the charge of the H atoms is 0.424e. To model surface 2, we take into account that at  
4  
5 low pHs there will be a large number of H atoms available to interact with the surface. The  
6  
7 following or a similar process will happen readily:  
8



11  
12 i.e. a proton from the acidic solution will interact with a hydroxyl group at the surface and  
13  
14 form a water molecule, which will then move into the solution. Once the surface is dried, this  
15  
16 water molecule is removed from the surface and our model of a  $\text{TiO}_2$  surface in acidic conditions  
17  
18 will have a positive charge of +1e left in the surface. Since the charge of the hydroxyl group  
19  
20 removed from the surface is only -0.424e, there will be an additional +0.576e to be distributed  
21  
22 among the atoms of the surface. This charge was distributed among the surface atoms as shown in  
23  
24 Table 3. Surface 3 is created taking into account a different process occurring in the basic solution.  
25  
26 Since under these conditions there is a large amount of  $\text{OH}^-$  groups, the following process will take  
27  
28 place:  
29



32  
33  
34 Thus, the result of the interaction between the hydroxylated surface and the  $\text{OH}^-$  species  
35  
36 from the solution is the removal of one proton from the surface to form a water molecule. This  
37  
38 water molecule will be removed into the basic solution, leaving a bridging O at the surface and a  
39  
40 charge of -1e, distributed among the atoms as shown in Table 3. Processes 1) and 2) are similar to  
41  
42 the common mechanisms considered within the PZC theory of oxides<sup>15</sup>.

43  
44 3.2.1. Adsorption of rhodamine 6G.  
45  
46  
47  
48  
49  
50  
51  
52  
53  
54  
55  
56  
57  
58  
59  
60

Deleted: 4

Deleted: 1

1  
2  
3  
4  
5  
6  
7  
8  
9  
10  
11  
12  
13  
14  
15  
16  
17  
18  
19  
20  
21  
22  
23  
24  
25  
26  
27  
28  
29  
30  
31  
32  
33  
34  
35  
36  
37  
38  
39  
40  
41  
42  
43  
44  
45  
46  
47  
48  
49  
50  
51  
52  
53  
54  
55  
56  
57  
58  
59  
60

The UV-vis spectra shown in a suggest that the maximum adsorption of rhodamine 6G molecules will occur under basic conditions. This experimental behaviour is not unexpected, since these dye molecules are positively charged, and there will be an electrostatic attraction between this charge and the negative charge present on the surface due to the basic solution. As the pH decreases, the amount of negative charges on the surface decreases, and therefore the adsorption decreases. When the pH is below the PZC, the surface is positively charged, a situation that must produce an electrostatic repulsion between the positive charge of the rhodamine molecule and the positive charges on the surface induced by the proton adsorbed from the acidic solutions. This general trend is also observed in the simulations. Figure 5 shows a snapshot of the simulation of the adsorption of rhodamine 6G on a fully hydroxylated surface, modelling the surface for neutral conditions. As shown in Table 4 (where the values of the energies of adsorption of the two rhodamine molecules on the four types of surfaces are shown), under basic conditions the adsorption energy of rhodamine 6G is -46.5 kcal/mol. Under neutral conditions  $E_{ad}$  decreases to -28.6 kcal/mol, and under acidic conditions it decreases further to -7.1 kcal/mol. The latter value is negative, suggesting that there might be some adsorption of rhodamine 6G under acidic conditions, in disagreement with what is experimentally observed. This apparent contradiction might be due to the simplicity of the model.  $E_{ad}$  is calculated as the difference in energy between two states. One state consists of two systems, the isolated  $TiO_2$  surface and the isolated rhodamine molecule. The other state consists of the rhodamine molecule adsorbed onto the surface. A more accurate value of  $E_{ad}$  would be obtained if the interaction of the rhodamine molecule with water molecules would have been taken into account accurately. The interaction rhodamine-water would cause a decrease of the adsorption energies of the two rhodamine molecules under all pH conditions. For this reason, this initial study only provides qualitative information about the

1 general trends of adsorption energy, predicting relative energetic differences, not the actual  
2 absolute values of adsorption energy.  
3  
4

5  
6 The dynamics of the rhodamine 6G molecule adsorbed onto the different surfaces shows  
7 significant variations.  
8  
9

10 In Figure 6 the values of the (x,y) coordinates of some relevant atoms of the molecule are  
11 plotted. The shape of the cell (from a top view) is also shown. In Figure 6a we can see the (x,y)  
12 values of the atom H7 of the rhodamine 6G when adsorbed on the bare, non-hydroxylated surface.  
13 The adsorption energy, in that case -51.0 kcal/mol, is higher than that of the other three cases in  
14 which the surface is hydroxylated. But there are no experimental results to be compared with  
15 these data, since bare TiO<sub>2</sub> surfaces are quickly hydrated and hydroxylated. The set of points are  
16 scattered over a wide range of values, indicating that the attraction between the molecule and the  
17 surface is evenly distributed over the surface, i.e. it is very easy for the molecule to hop around the  
18 surface. Under basic conditions we observe the opposite effect: there is a strong attraction towards  
19 the negatively charged surface defect, a feature which creates a preference for the molecule to stay  
20 around it. In Figure 6b we see the (x,y) values of the atoms O1 and H7, as well as the position of  
21 the O atom that has lost its H due to the basic solution. The positions of the O1 and H7 atoms are  
22 localised in small areas, indicating that the molecule does not diffuse easily once it is absorbed.  
23 Under neutral conditions (Figure 6c) the mobility of the molecule is higher, and E<sub>ad</sub> is lower, -28.6  
24 kcal/mol, a result that agrees with the experimental observations. Under acidic conditions the  
25 mobility is still higher, as suggested by the scattered set of points corresponding to the movement  
26 of the H7 atom (Figure 6d). The molecule moves around the Ti atom which has lost its hydroxyl  
27 group, and is part of the positively charged defect. During the simulation, the phenyl moiety of the  
28 rhodamine 6G molecule is often inserted within the region previously occupied by the hydroxyl  
29 group. E<sub>ad</sub> is now -7.1 kcal/mol, a value which is much smaller than in the case of adsorption  
30  
31  
32  
33  
34  
35  
36  
37  
38  
39  
40  
41  
42  
43  
44  
45  
46  
47  
48  
49

1 under neutral conditions. The most relevant geometric parameters that describe the adsorption of  
2 the rhodamine 6G molecules are the angles  $\alpha$  and  $\beta$ .  $\alpha$  is defined as the angle between the axis **a** of  
3 the molecules (which is shown in Figure 2), and the **z** axis of the unit cell. Analogously,  $\beta$  is the  
4 angle between the molecular axis **b** and the **z** axis. A value of  $90^\circ$  in both angles would correspond  
5 to an adsorption geometry in which the molecule lies parallel to the surface. The convention we  
6 have used to calculate the angles means that an angle lower than  $90^\circ$  implies that the  
7 corresponding molecular axis (**a** or **b**) points upwards, and viceversa. Figure 7 shows the values of  
8 the angles  $\alpha$  and  $\beta$  during the simulations, for the two rhodamine molecules at the four conditions  
9 of pH studied.

10  
11 The average values for the whole simulations are shown in Figure 8. For rhodamine 6G the  
12 average value of the angle  $\alpha$  is very close to  $90^\circ$  in all cases. The larger deviation is found for the  
13 adsorption under basic conditions. The value of  $88^\circ$  obtained suggests an adsorption almost  
14 parallel to the surface. The angle  $\beta$  is more affected by the presence of the phenyl group, which has  
15 the effect of decreasing the adsorption angle of the molecule. As a result, the average value of the  
16 angle  $\beta$  ranges from  $80.7^\circ$ , in the case of non-hydroxylated surface, to  $84.0^\circ$  for the adsorption  
17 under acidic conditions. This higher angle for acidic conditions is due to the mentioned ability of  
18 the molecule to introduce the phenyl moiety within the region previously occupied by the removed  
19 hydroxyl group, a feature which permits a more parallel adsorption.

### 3.2.2. Adsorption of rhodamine 800.

20  
21 The experimental observations suggest that the adsorption of rhodamine 800 is less  
22 affected than the rhodamine 6G by changes in the pH of the surface, although the maximum  
23 adsorption also takes place under basic conditions and the minimum under acidic conditions. The

Deleted: 4

1 values of the energies of adsorption calculated from the simulations for basic, neutral and acidic  
2 conditions are -51.6 kcal/mol, -33.2 kcal/mol and -29.4 kcal/mol respectively. The difference  
3 between the energies for neutral and acidic conditions is just 3.8 kcal/mol, almost five times  
4 smaller than the difference between the values for neutral and basic conditions, which is 18.4  
5 kcal/mol. This effect is in agreement with the observation that a low pH only produces a small  
6 decrease in the intensity of the UV-vis adsorption bands (see b). The simulations provide some  
7 hints to understand the reasons for this behaviour. As it happens for rhodamine 6G, under basic  
8 conditions  $E_{ad}$  is higher because the negative charge of the **surface site defect** modelling the basic  
9 conditions attracts the positive charge of the molecule. The N atom of the nitrile group of the  
10 rhodamine R800 molecule (N3 in Figure 2b) has a negative charge of -0.417e. Therefore, the  
11 negatively charged **site** at the surface interacts preferentially with the opposite side of the  
12 molecule, where most of the positive charge of the molecule is concentrated. It can be observed in  
13 Figure 6f that the N atom does not get close to the surface O atom. To represent the movement of  
14 the xanthene moiety we have chosen the atom O1. It has a small negative charge (-0.183e), and is  
15 surrounded by positive charges, so the position of the O1 atom is oscillating around the surface O  
16 atom. **Regarding** Looking to the angles accounting for this interaction, the average values of both  
17 angles  $\alpha$  and  $\beta$  are within the range  $90^\circ$ - $92^\circ$  (see Figure 8), which means that the molecule is  
18 basically lying parallel to the surface.

19  
20  
21  
22  
23  
24  
25  
26  
27  
28  
29  
30  
31  
32  
33  
34  
35  
36  
37  
38  
39  
40  
41  
42  
43  
44  
45  
46  
47  
48  
49  
50  
51  
52  
53  
54  
55  
56  
57  
58  
59  
60

In the surface that models neutral conditions the negatively charged **site defect** is not present, and the interaction between the rhodamine molecule and the surface is mainly due to their mutual van der Waals interactions. As a result,  $E_{ad}$  decreases from -51.6 kcal/mol to -33.2 kcal/mol. The negatively charged N atom in the nitrile group is now mainly attracted to the positively charged H atoms of the hydroxyl groups, and falls in the potential well created by the H atoms belonging to three adjacent hydroxyl groups. This can be seen in Figure 6g, where we have

1 plotted the coordinates of the atoms N3 and O1 of the rhodamine 800 molecules, as well as the  
2  
3 coordinates of the O atoms of the hydroxyl groups, which are less mobile than the H atoms with  
4  
5 which they are bonded. The distance from the superficial H atoms to the centre of the xanthene  
6  
7 moiety, 2.82 Å, is roughly the same as in the case of adsorption under basic conditions, and the  
8  
9 adsorption geometry in both cases is very similar. This similarity is also found for the values of the  
10  
11 angles  $\alpha$  and  $\beta$ , which lie within a range of 90°-92° (Figure 7g and Figure 8), thus indicating that  
12  
13 the adsorption is parallel to the surface.  
14

15  
16 Experimentally, the relatively high adsorption of rhodamine 800 under acidic conditions  
17  
18 (which is very similar to the level of adsorption in neutral conditions) is somewhat unexpected,  
19  
20 because under these conditions, both the surface and the rhodamine 800 molecule are positively  
21  
22 charged. Our simulations provide a basis to understand why a significant adsorption takes place.  
23  
24 The value of  $E_{ad}$  predicted by our simulations is -29.4 kcal/mol, which is very close to the value  
25  
26 obtained under neutral conditions, -33.2 kcal/mol. The reason why the electrostatic repulsion  
27  
28 between the two charged systems does not produce a significant decrease in the value of  $E_{ad}$  is due  
29  
30 to the fact that the positive charge around the Ti atom at the surface does not interact directly with  
31  
32 the positive charge of the rhodamine molecule. Instead, it is the negatively charged N atom of the  
33  
34 nitrile group the one that is closer to it. Figure 6h shows that the positively charged region of the  
35  
36 molecule (which surrounds the O1 atom) stays as far away as possible from the Ti atom, whereas  
37  
38 the N3 atom is attracted by the positive charge of the Ti atom. There is a change in the angles of  
39  
40 adsorption respect to the cases of basic and neutral conditions. The average value of the angle  $\alpha$ ,  
41  
42 90°, is similar to the previous cases, but the average value of the angle  $\beta$  has increased to 95°  
43  
44 (Figure 7h and Figure 8). This is due to the mentioned attraction between the N3 atom and the  
45  
46 surface Ti atom, which tends to keep them together. Indeed, this attraction induces a decrease of  
47  
48 the distance between the molecule and surface (which changes from 2.8 Å to 2.7 Å). Since the rest  
49  
50

1 of the molecule cannot get closer to the hydroxyl groups of the surface, this effect results in an  
2 increase of the adsorption angle  $\beta$ , i.e. the position of the N3 atom is lower than that of the rest of  
3 the molecule. This particular geometrical arrangement has the net effect of creating an attraction  
4 between two positively charged systems.  
5  
6  
7  
8  
9

#### 10 11 12 13 14 15 16 17 18 19 **4. Concluding remarks**

Deleted: 5

20  
21 The simulations reported here offer a preliminary atomistic insight into the adsorption  
22 processes on TiO<sub>2</sub> of two industrially relevant dye molecules, namely rhodamine 6G and  
23 rhodamine 800. The task of simulating TiO<sub>2</sub> surfaces is very challenging. Theoretical studies of  
24 the adsorption of molecules are often carried out by employing bare TiO<sub>2</sub> surfaces. Our results  
25 show that there are large differences in adsorption energies and geometries when the state of the  
26 surface is changed. Thus, for the two studied molecules the adsorption energy on a hydroxylated  
27 surface is almost half of that calculated in the case of a bare surface. One of the greatest challenges  
28 regarding the simulation of TiO<sub>2</sub> surfaces is to model the effect of the different pHs. Using two  
29 models to simulate high and low pH conditions, we have calculated the adsorption energies of the  
30 two molecules under basic, neutral and acidic conditions. For rhodamine 6G the simulations  
31 predict a high energy of adsorption and therefore much adsorption under basic conditions, less  
32 adsorption under neutral conditions, and practically no adsorption under acidic conditions. For  
33 rhodamine 800 there is a high energy of adsorption under basic conditions, while the adsorption  
34 energies under neutral and acidic conditions are lower than the latter, but very similar to each  
35 other. These results are in qualitative agreement with the experimental observations, which  
36  
37  
38  
39  
40  
41  
42  
43  
44  
45  
46  
47  
48  
49

1 provides additional confidence on the ability of the simulations to model realistic adsorption  
2 conditions. However, despite this success in achieving a qualitative agreement between  
3 experimental and theoretical results, there are still many factors involved in the adsorption of  
4 molecules on TiO<sub>2</sub> which we have not taken into account. For example, we have studied the final  
5 states, in which the rhodamine molecules are adsorbed onto the dry surface, but we have not  
6 modelled the transition from the wet to the dry TiO<sub>2</sub> surface. This is an interesting process, since  
7 there is a loss of water molecules, while the rhodamine molecules are kept attached to the surface.  
8 Another relevant factor that influences the adsorption of rhodamine molecules is the presence of  
9 counterions<sup>43,45</sup>. On the other hand, there is a rich variety of ways in which rhodamine molecules  
10 can interact, both in solution and on the surface, such as forming monomers, H-dimers, J-dimers,  
11 etc<sup>6-11</sup>, which have a great influence on the photoluminescence properties<sup>21,46,47</sup>. Thus another  
12 interesting problem is to assess how the dimerisation process affects the adsorption on the surfaces.  
13 The ultimate goal of the inclusion of all these other effects would be to obtain a more accurate  
14 description of these systems, which could provide theoretical data to guide the experimental  
15 research. For these reasons an intense theoretical work is being carried out in our group along this  
16 line.

Deleted: 6

## 5. Acknowledgements

We dedicate this work to the memory of José Antonio Mejías, an excellent friend and good scientist, who put the first stones of this research line in our group. We will always remember him kindly. We thank the Ministry of Science and Education of Spain (project MAT 2007-65764/NAN2004-09317 and the CONSOLIDER INGENIO 2010-CSD2008-00023) and the Junta de Andalucía (projects TEP2275 and P07-FQM-03298) for financial support.

1  
2  
3  
4  
5  
6  
7  
8  
9  
10  
11  
12  
13  
14  
15  
16  
17  
18  
19  
20  
21  
22  
23  
24  
25  
26  
27  
28  
29  
30  
31  
32  
33  
34  
35  
36  
37  
38  
39  
40  
41  
42  
43  
44  
45  
46  
47  
48  
49  
50  
51  
52  
53  
54  
55  
56  
57  
58  
59  
60

For Peer Review Only

	Dye concentration [ mol cm <sup>-2</sup> nm <sup>-1</sup> 10 <sup>-12</sup> ]		
	pH =3.8	pH=5.5	pH=6.6
TiO <sub>2</sub> -Rh6G	0	2.87	13.07
TiO <sub>2</sub> -Rh800	5.82	4.12	7.85

Table 1

Concentration of the adsorbed dyes in the porous TiO<sub>2</sub> thin films as a function of the pH.

	Torsional angle 10-1-4-5	Dist. 1-2	Dist 2-3	Dist. 4-5	Dist. 5-11	Angle 1-4-5	Angle 1-2-3
Predota et al. <sup>23,28</sup>	126.2°	1.93Å	1.01Å	0.97Å	2.73Å	127.8°	119.8°
Plus added terms.							
DFT	122.3°	1.87Å	0.98Å	0.98Å	2.49Å	126.2°	118.3°

Table 2

Values of some of the important geometrical features of the (101) hydroxylated anatase surface, obtained with DFT and with the interatomic potentials developed by Predota et al.<sup>23,28</sup>, including the new terms that improve the description of the O-H bonds for this particular surface.

Deleted: ¶  
Atom name ... [2]

Atom	Charge in basic conditions	Charge in neutral conditions	Charge in acidic conditions
1-Ti	2.124	2,196	2.268
2-O	-0.920	-0,848	No atom
3-H	0.352	0,424	No atom
4-O	-1.170	-1,098	-1.026
5-H	No atom	0,424	0.496
6-O	-1.170	-1,098	-1.026
7-O	-1.170	-1,098	-1.026
8-O	-1.170	-1,098	-1.026
9-Ti	2.124	2,196	2.268
10-O	-1,098	-1,098	-1.026

**Table 3**

Charges of all the atoms involved in the defects appearing at high and low pH, as well as the charges of the atoms of the hydroxylated surface under neutral conditions.

1  
2  
3  
4  
5  
6  
7  
8  
9  
10  
11  
12  
13  
14  
15  
16  
17  
18  
19  
20  
21  
22  
23  
24  
25  
26  
27  
28  
29  
30  
31  
32  
33  
34  
35  
36  
37  
38  
39  
40  
41  
42  
43  
44  
45  
46  
47  
48  
49  
50  
51  
52  
53  
54  
55  
56  
57  
58  
59  
60

	Acidic	Neutral	Basic	Non-hydroxilated
<b>Rhodamine 6G</b>	<b>-7.1</b>	<b>-28.6</b>	<b>-46.5</b>	<b>-51.0</b>
<b>Rhodamine 800</b>	<b>-29.4</b>	<b>-33.2</b>	<b>-51.6</b>	<b>-56.7</b>

**Table 4**

Energies of adsorption,  $E_{ad}$ , of the two rhodamine molecules studied on the (101) surface of anatase. All energies are in kcal/mol.

For Peer Review Only

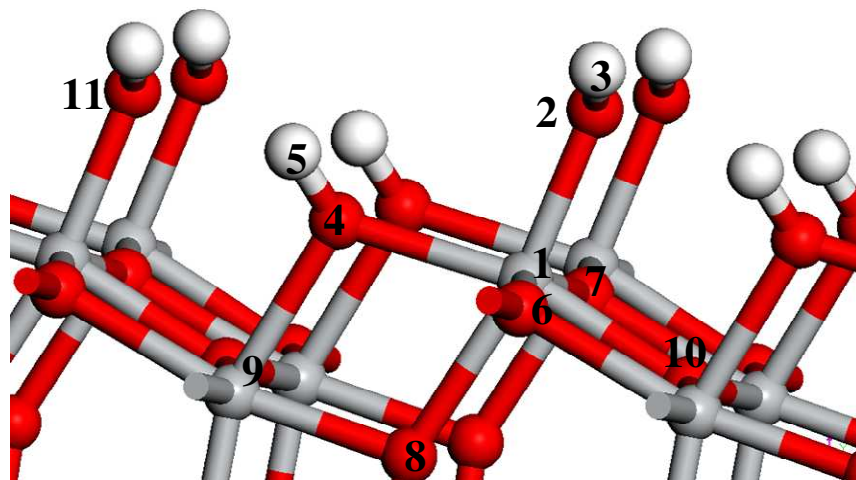
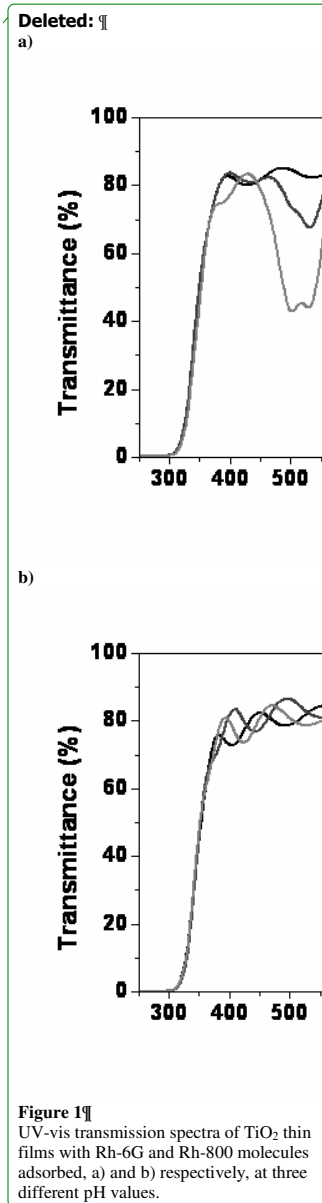
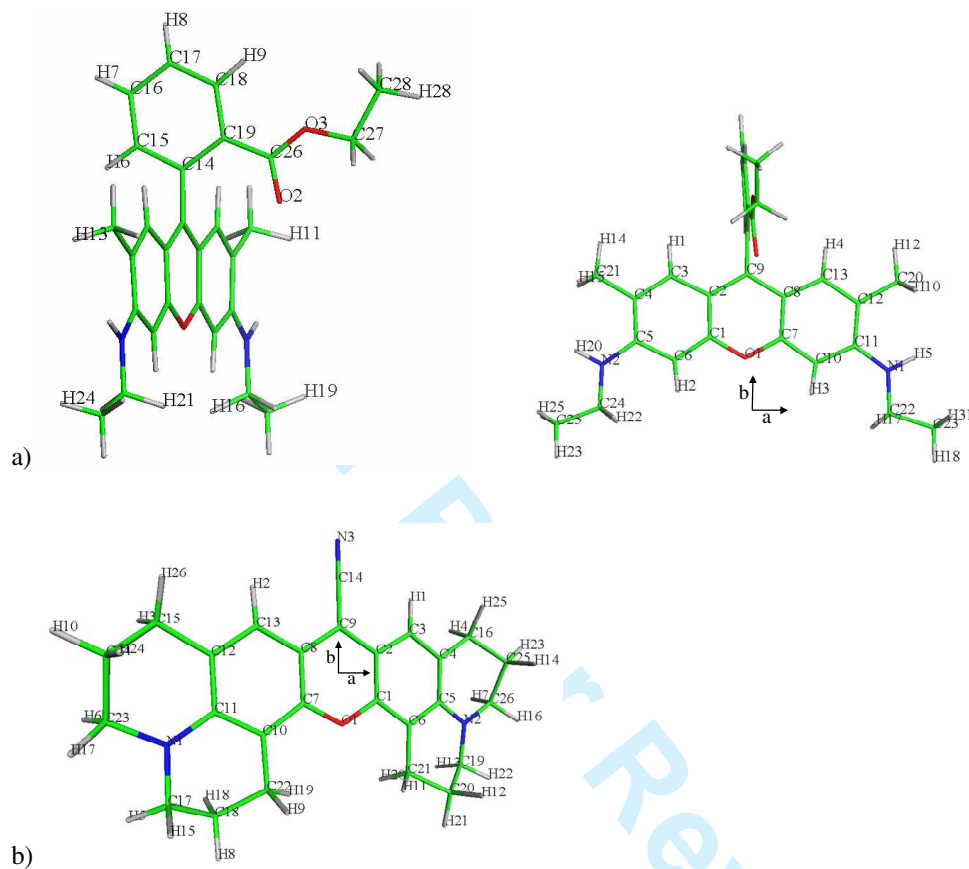


Figure 1

Close view of the hydroxylated (101) anatase surface. Red balls represent O atoms, grey balls represent Ti atoms and white balls represent H atoms.





34 **Figure 2**

35  
36 a) Two views of a rhodamine 6G molecule. b) A view of a rhodamine 800 molecule. The figures  
37 show the numbering assigned to each atom, which are used to assign the force field atom types and  
38 charges in **SI Table 1 and SI Table 2**. The molecular axis **a** and **b** are also shown. In both figures  
39 green, blue, red and white sticks represent C, N, O and H atoms respectively.

Deleted: and

Formatted: Font: Bold

Formatted: Font: Bold

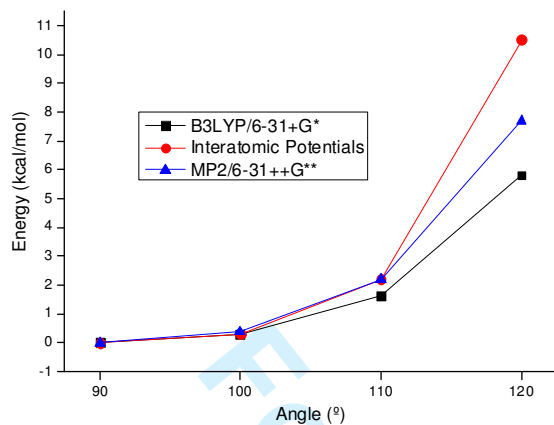
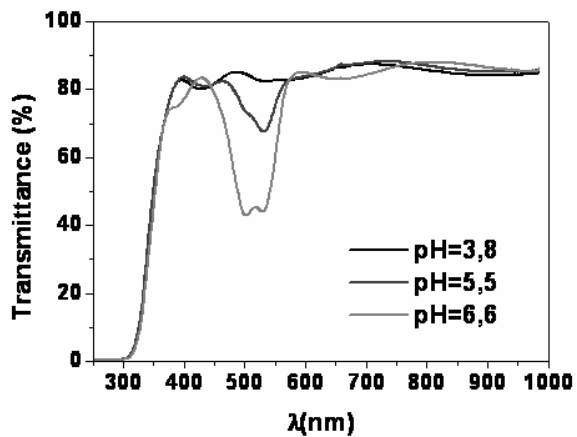
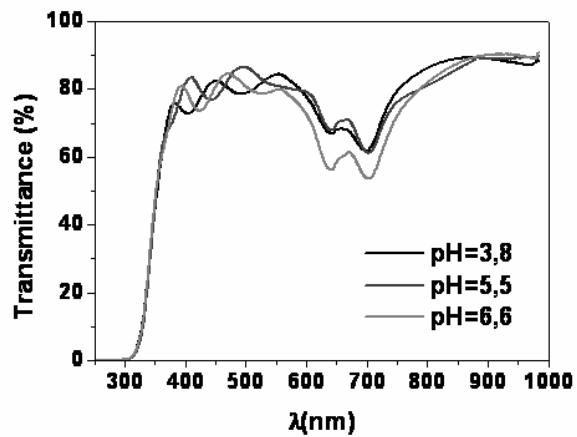


**Figure 3**

Change in energy as the angle between the xanthene and phenyl moieties is changed, calculated with two *ab initio* methods (B3LYP/6-31+G\* and MP2/6-31++G\*\*) and with the classical interatomic potentials used in this study.



a)

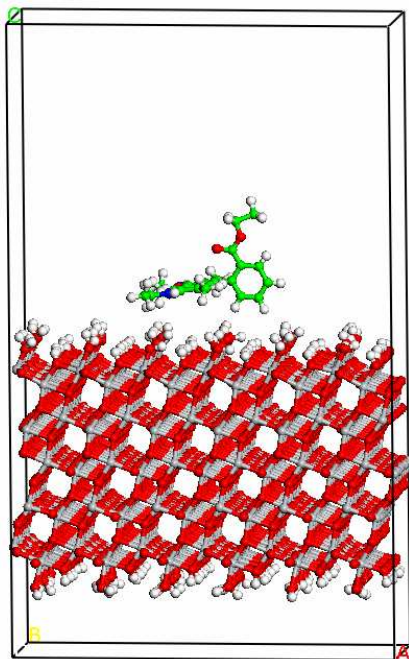


b)

Figure 4

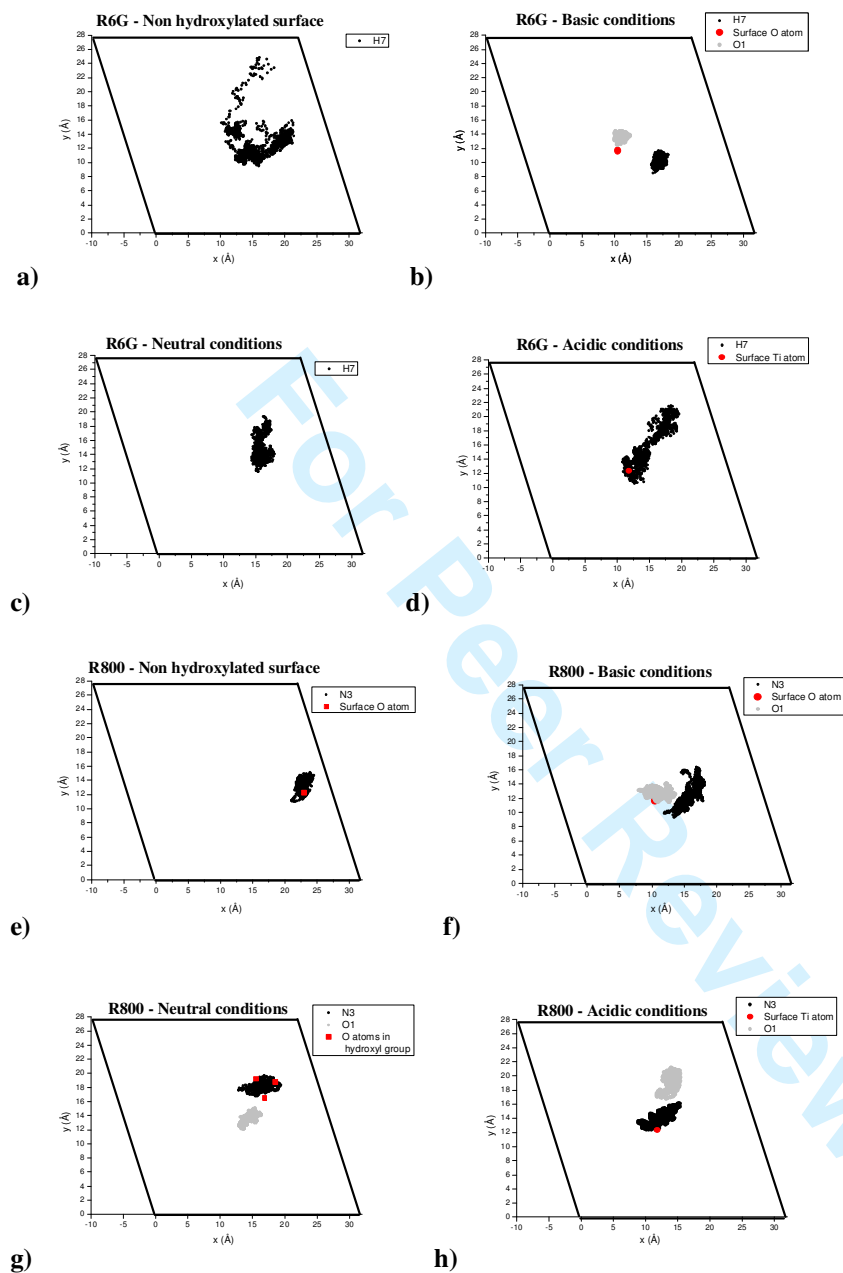
40  
41  
42  
43  
44  
45  
46  
47  
48  
49  
50  
51  
52  
53  
54  
55  
56  
57  
58  
59  
60

UV-vis transmission spectra of TiO<sub>2</sub> thin films with Rh-6G and Rh-800 molecules adsorbed, a) and b) respectively, at three different pH values.



**Figure 5**

Ball and stick view of the simulation cell used to study the adsorption of rhodamine 6G in a fully hydroxylated surface, under neutral pH conditions. Green, blue, red, white and grey balls atoms represent C, N, O, H and Ti atoms respectively.

**Figure 6**

Plot of the values of the (x,y) coordinates of some relevant atoms, taken every 0.1 ps during the whole simulations. a) R6G on non-hydroxylated surface, b) R6G under basic conditions, c) R6G under neutral conditions, d) R6G under acidic conditions, e) R800 on non-hydroxylated surface, f) R800 under basic conditions, g) R800 under neutral conditions, h) R800 under acidic conditions.

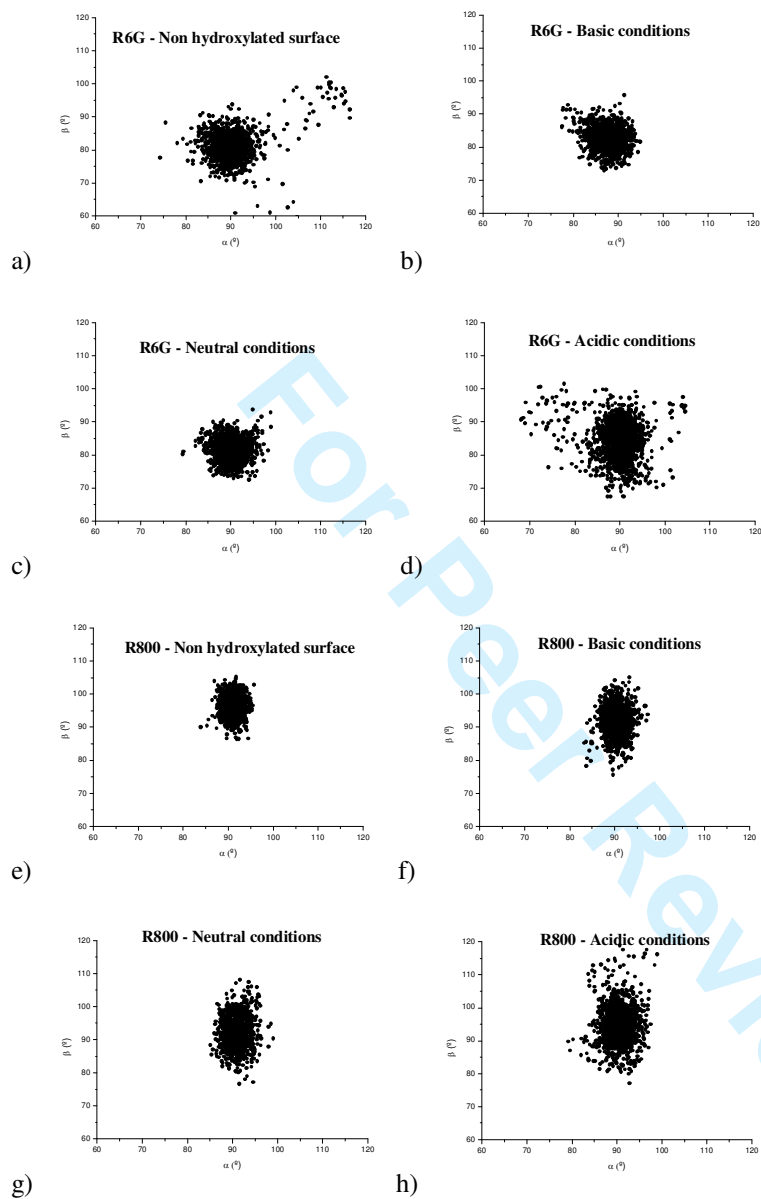


**Figure 7**

Values of the angles  $\alpha$  and  $\beta$  during the simulations for the different simulations.  $\alpha$  ( $\beta$ ) is defined as the angle between the axis **a** (**b**) of the molecules (which is shown in Figure 2), and the **z** axis of the unit cell. a) R6G on non-hydroxylated surface, b) R6G under basic conditions, c) R6G under neutral conditions, d) R6G under acidic conditions, e) R800 on non-hydroxylated surface, f) R800 under basic conditions, g) R800 under neutral conditions, h) R800 under acidic conditions.

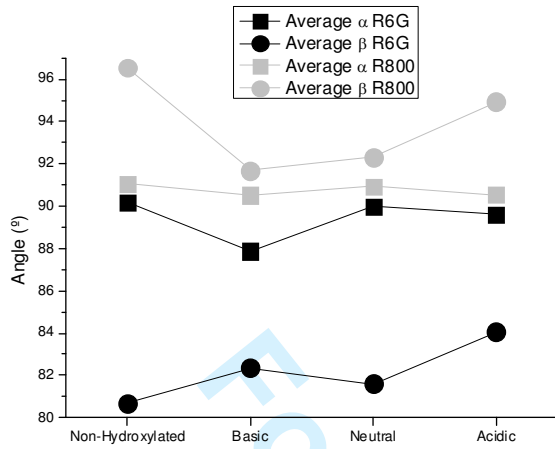


**Figure 8**  
Average values of the angles  $\alpha$  and  $\beta$  during the simulations.

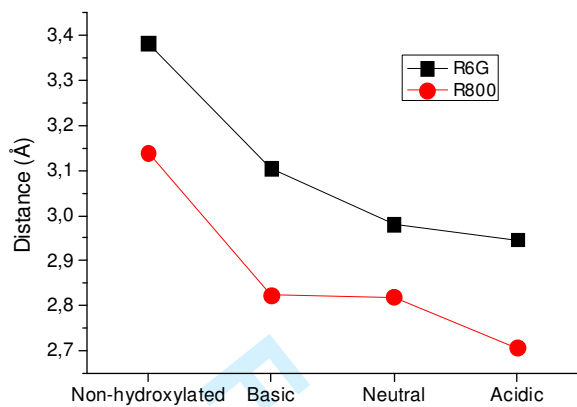


**Figure 9**

Average distance between the surfaces and the rhodamine molecules.

## Supplementary Information

Atom name	Force Field type	Charge	Atom name	Force Field type	Charge
C1	C R	0.48	O3	O 2	-0.46
C2	C R	-0.139	C27	C 3	0.346
C3	C R	-0.287	C28	C 3	-0.25
C4	C R	0.114	H1	H	0.173
C5	C R	0.287	H2	H	0.231
C6	C R	-0.438	H3	H	0.238
O1	O R	-0.385	H4	H	0.17
C7	C R	0.487	H5	H HB	0.365
C8	C R	-0.136	H6	H	0.139
C9	C R	0.08	H7	H	0.15
C10	C R	-0.46	H8	H	0.155
C11	C R	0.31	H9	H	0.148
C12	C R	0.106	H10	H	0.089
C13	C R	-0.285	H11	H	0.123
N1	N R	-0.534	H12	H	0.083
C14	C R	0.428	H13	H	0.125
C15	C R	-0.298	H14	H	0.093
C16	C R	-0.058	H15	H	0.089
C17	C R	-0.161	H16	H	0.045
C18	C R	-0.083	H17	H	0.054
C19	C R	-0.302	H18	H	0.079
C20	C 3	-0.286	H19	H	0.087
C21	C 3	-0.303	H20	H HB	0.357
C22	C 3	0.166	H21	H	0.063
C23	C 3	-0.232	H22	H	0.041
N2	N R	-0.521	H23	H	0.033
C24	C 3	0.205	H24	H	0.079
C25	C 3	-0.242	H25	H	0.061
C26	C 2	0.784	H26	H	0.088
O2	O 1	-0.532	H27	H	-0.001
O3	O 2	-0.46	H28	H	0.002
C27	C 3	0.346	H29	H	0.071
C28	C 3	-0.25	H30	H	0.084
H1	H	0.173	H31	H	0.085

SI Table 1

Atomic charges and DREIDING force field types of the atoms of rhodamine 6G shown in Figure 2a.

Atom name	Force Field type	Charge	Atom name	Force Field type	Charge
C1	C R	0.18	H3	H	0.074
C2	C R	0.057	C24	C 3	-0.008
C3	C R	-0.365	H4	H	0.078
C4	C R	0.181	C25	C 3	0.046
C5	C R	-0.061	C26	C 3	-0.161
C6	C R	-0.058	N3	N 1	-0.417
O1	O R	-0.183	H5	H	0.059
C7	C R	0.242	H6	H	0.069
C8	C R	0.033	H7	H	0.094
C9	C R	-0.064	H8	H	0.055
C10	C R	-0.137	H9	H	0.054
C11	C R	0.005	H10	H	0.053
C12	C R	0.14	H11	H	0.029
C13	C R	-0.344	H12	H	0.038
N1	N R	-0.002	H13	H	0.09
C14	C 1	0.417	H14	H	0.028
C15	C 3	-0.131	H15	H	0.074
C16	C 3	-0.137	H16	H	0.1
C17	C 3	-0.016	H17	H	0.05
C18	C 3	-0.06	H18	H	0.058
N2	N R	0.085	H19	H	0.027
C19	C 3	-0.143	H20	H	0.059
C20	C 3	0.016	H21	H	0.042
H1	H	0.211	H22	H	0.098
C21	C 3	-0.017	H23	H	0.048
C22	C 3	0.018	H24	H	0.043
H2	H	0.209	H25	H	0.075
C23	C 3	-0.011	H26	H	0.082

Formatted: Indent: Before: 0 pt,  
Hanging: 36 pt

### SI Table 2

Atomic charges and DREIDING force field types of the atoms of rhodamine 800 shown in Figure 2b.

## Bibliography

- (1) R. Sasai; N. Iyi; T. Fujita; F.L. Arbeloa; Martinez; K. Takagi; H. Itoh. Luminescence Properties of Rhodamine 6G Intercalated in Surfactant/Clay Hybrid Thin Solid Films. *Langmuir*, 20, 4715 (2004)
- (2) F. Marlow; M.D. McGehee; D. Zhao; B.F. Chmelka; G.D. Stucky. Doped Mesoporous Silica Fibers: A New Laser Material. *Advanced Materials*, 11, 632 (1999)
- (3) D. Tleugabulova; Z. Zhang; Y. Chen; M.A. Brook; J.D. Brennan. Fluorescence Anisotropy in Studies of Solute Interactions with Covalently Modified Colloidal Silica Nanoparticles. *Langmuir*, 20, 848 (2004)
- (4) L. Bahadur; P. Srivastava. Efficient photon-to-electron conversion with rhodamine 6G-sensitized nanocrystalline n-ZnO thin film electrodes in acetonitrile solution. *Solar Energy Materials and Solar Cells*, 79, 235 (2003)
- (5) T. Ohishi. An ethoxy-silano rhodamine B derivative and its application to surface coatings on display devices. *Journal of Non-Crystalline Solids*, 332, 80 (2003)
- (6) V. Martínez Martínez; F. López Arbeloa; J. Bañuelos Prieto; T. Arbeloa Lopez; I. López Arbeloa. Characterization of Supported Solid Thin Films of Laponite Clay. Intercalation of Rhodamine 6G Laser Dye. *Langmuir*, 20, 5709 (2004)
- (7) A.H. Gemeay. Adsorption Characteristics and the Kinetics of the Cation Exchange of Rhodamine-6G with Na<sup>+</sup>-Montmorillonite. *Journal of Colloid and Interface Science*, 251, 235 (2002)
- (8) J. Bujdák; N. Iyi; R. Sasai. Spectral Properties, Formation of Dye Molecular Aggregates, and Reactions in Rhodamine 6G/Layered Silicate Dispersions. *The Journal of Physical Chemistry B*, 108, 4470 (2004)
- (9) J. Bujdák; N. Iyi. Molecular Orientation of Rhodamine Dyes on Surfaces of Layered Silicates. *The Journal of Physical Chemistry B*, 109, 4608 (2005)
- (10) V. Martínez; S. Salleres; J. Bañuelos; F.L. Arbeloa. Application of Fluorescence with Polarized Light to Evaluate the Orientation of Dyes Adsorbed in Layered Materials. *Journal of Fluorescence*, 16, 233 (2006)
- (11) F. del Monte; J.D. Mackenzie; D. Levy. Rhodamine fluorescent dimers adsorbed on the porous surface of silica gels. *Langmuir*, 16, 7377 (2000)
- (12) A. Barranco; P. Groening. Fluorescent Plasma Nanocomposite Thin Films Containing Nonaggregated Rhodamine 6G Laser Dye Molecules. *Langmuir*, 22, 6719 (2006)
- (13) R. Vogel; P. Meredith; I. Kartini; M. Harvey; J.D. Riches; A. Bishop; N. Heckenberg; M. Trau; H. Rubinsztein-Dunlop. Mesostructured Dye-Doped Titanium Dioxide for Micro-Optoelectronic Applications. *ChemPhysChem*, 4, 595 (2003)
- (14) J.R. Sánchez-Valencia; A. Borrás; A. Barranco; V.J. Rico; J.P. Espinós; A.R. González-Elipe. Preillumination of TiO<sub>2</sub> and Ta<sub>2</sub>O<sub>5</sub> Photoactive Thin Films As a Tool to Tailor the Synthesis of Composite Materials. *Langmuir*, 24, 9460 (2008)
- (15) M. Kosmulski *Chemical Properties of Material Surfaces*; Marcel Dekker Inc., 2001.
- (16) B. O'Regan; M. Grätzel. *Nature*, 353, 737 (1991)
- (17) A. Hagfeldt; M. Grätzel. *Chemical Reviews*, 95, 49 (1995)
- (18) F. de Angelis; S. Fantacci; A. Selloni; M.K. Nazeeruddin; M. Grätzel. Time-Dependent Density Functional Theory Investigations on the Excited States of Ru(II)-Dye-

- 1 Sensitized TiO<sub>2</sub> Nanoparticles: The Role of Sensitizer Protonation. *Journal of the American*  
2 *Chemical Society*, 129, 14156 (2007)
- 3 (19) S.A. Tomás; S. Stolik; R. Palomino; R. Lozada; C. Persson; I. Pepe; A.  
4 Ferreira da Silva. Influence of rhodamine 6G doping on the optical properties of TiO<sub>2</sub> sol-gel  
5 films. *Journal of Applied Physics*, 98, 073516 (2005)
- 6 (20) R. Sasai; T. Fujita; N. Iyi; H. Itoh; K. Takagi. Aggregated Structures of  
7 Rhodamine 6G Intercalated in a Fluor-Taeniolite Thin Film. *Langmuir*, 18, 6578 (2002)
- 8 (21) J. Bujdák; N. Iyi. Molecular Aggregation of Rhodamine Dyes in Dispersions of  
9 Layered Silicates: Influence of Dye Molecular Structure and Silicate Properties. *The Journal*  
10 *of Physical Chemistry B*, 110, 2180 (2006)
- 11 (22) K. Robbie; M.J. Brett. Sculptured thin films and glancing angle deposition:  
12 Growth mechanics and applications. *J. Vac. Sci. Technol. A*, 15, 1460 (1997)
- 13 (23) M. Predota; A.V. Bandura; P.T. Cummings; J.D. Kubicki; D.J. Wesolowski;  
14 A.A. Chialvo; M.L. Machesky. Electric Double Layer at the Rutile (110) Surface. 1.  
15 Structure of Surfaces and Interfacial Water from Molecular Dynamics by Use of ab Initio  
16 Potentials. *The Journal of Physical Chemistry B*, 108, 12049 (2004)
- 17 (24) A. Fortunelli; S. Monti. Simulations of Lipid Adsorption on TiO<sub>2</sub> Surfaces in  
18 Solution. *Langmuir*, 24, 10145 (2008)
- 19 (25) S. Köppen; O. Bronkalla; W. Langel. Adsorption Configurations and Energies  
20 of Amino Acids on Anatase and Rutile Surfaces. *The Journal of Physical Chemistry C*, 112,  
21 13600 (2008)
- 22 (26) A. Tilocca; A. Selloni. Methanol Adsorption and Reactivity on Clean and  
23 Hydroxylated Anatase(101) Surfaces. *Journal of Physical Chemistry B*, 108, 19314 (2004)
- 24 (27) A. Tilocca; C. Di Valentin; A. Selloni. O<sub>2</sub> Interaction and Reactivity on a  
25 Model Hydroxylated Rutile(110) Surface. *The Journal of Physical Chemistry B*, 109, 20963  
26 (2005)
- 27 (28) A.V. Bandura; J.D. Kubicki. Derivation of Force Field Parameters for TiO<sub>2</sub>-  
28 H<sub>2</sub>O Systems from ab Initio Calculations. *Journal of Physical Chemistry B*, 107, 11072 (2003)
- 29 (29) M. Matsui; M. Akaogi. Molecular dynamics simulation of the structural and  
30 physical properties of the four polymorphs of TiO<sub>2</sub>. *Molecular Simulation*, 6, 239 (1991)
- 31 (30) G. Kresse; J. Joubert. *Physical Review B*, 59, 1758 (1999)
- 32 (31) J. Perdew; J. Chevary; S. Vosko; K. Jackson; M. Pederson; D. Singh; C.  
33 Fiolhais. *Physical Review B*, 46, 6671 (1992)
- 34 (32) G. Kresse; J. Hafner. *Physical Review B*, 47, 558 (1993)
- 35 (33) G. Kresse; J. Furthmuller. *Physical Review B*, 54, 11169 (1996)
- 36 (34) G. Kresse; J. Furthmuller. *Computational Materials Science*, 6, 15 (1996)
- 37 (35) H.J. Monkhorst; J.D. Pack. *Physical Review B*, 13, 5188 (1976)
- 38 (36) S.L. Mayo; B.D. Olafson; W.A. Goddard. DREIDING: a generic force field for  
39 molecular simulations. *The Journal of Physical Chemistry*, 94, 8897 (1990)
- 40 (37) D.E. Williams; S.R. Cox. Nonbonded Potentials for Azahydrocarbons: the  
41 Importance of the Coulombic Interaction. *Acta Cryst. B* 40, 414 (1984)
- 42 (38) D.E. Williams; D.J. Houpt. Fluorine Nonbonded Potential Parameters Derived  
43 from Crystalline Perfluorocarbons. *Acta Cryst. B* 42, 286 (1986)
- 44 (39) U.C. Singh; P.A. Kollman. *J. Comp. Chem.*, 5, 129 (1984)
- 45 (40) B.H. Besler; K.M. Merz Jr; P.A. Kollman. *J. Comp. Chem.*, 11, 431 (1990)
- 46 (41) M.J. Frisch; G.W. Trucks; H.B. Schlegel; G.E. Scuseria; M.A. Robb; J.R.  
47 Cheeseman; J.A.M. Jr.; T. Vreven; K.N. Kudin; J.C. Burant; J.M. Millam; S.S. Iyengar; J.  
48 Tomasi; V. Barone; B. Mennucci; M. Cossi; G. Scalmani; N. Rega; G.A. Petersson; H.

1  
2  
3  
4  
5  
6  
7  
8  
9  
10  
11  
12  
13  
14  
15  
16  
17  
18  
19  
20  
21  
22  
23  
24  
25  
26  
27  
28  
29  
30  
31  
32  
33  
34  
35  
36  
37  
38  
39  
40  
41  
42  
43  
44  
45  
46  
47  
48  
49  
50  
51  
52  
53  
54  
55  
56  
57  
58  
59  
60

Nakatsuji; M. Hada; M. Ehara; K. Toyota; R. Fukuda; J. Hasegawa; M. Ishida; T. Nakajima; Y. Honda; O. Kitao; H. Nakai; M. Klene; X. Li; J.E. Knox; H.P. Hratchian; J.B. Cross; V. Bakken; C. Adamo; J. Jaramillo; R. Gomperts; R.E. Stratmann; O. Yazyev; A.J. Austin; R. Cammi; C. Pomelli; J.W. Ochterski; P.Y. Ayala; K. Morokuma; G.A. Voth; P. Salvador; J.J. Dannenberg; V.G. Zakrzewski; S. Dapprich; A.D. Daniels; M.C. Strain; O. Farkas; D.K. Malick; A.D. Rabuck; K. Raghavachari; J.B. Foresman; J.V. Ortiz; Q. Cui; A.G. Baboul; S. Clifford; J. Cioslowski; B.B. Stefanov; G. Liu; A. Liashenko; P. Piskorz; I. Komaromi; R.L. Martin; D.J. Fox; T. Keith; M.A. Al-Laham; C.Y. Peng; A. Nanayakkara; M. Challacombe; P.M.W. Gill; B. Johnson; W. Chen; M.W. Wong; C. Gonzalez; G. J. A. Pople, Inc., Wallingford CT. Gaussian 03, 2004.

(42) A.D. Becke. *J. Chem. Phys.*, **98**, 5648 (1993)

(43) P. Capková; P. Malý; M. Pospíšil; Z. Klika; H. Weissmannová; Z. Weiss. Effect of surface and interlayer structure on the fluorescence of rhodamine B-montmorillonite: modeling and experiment. *Journal of Colloid and Interface Science*, **277**, 128 (2004)

(44) J.D. Gale. GULP: A computer program for the symmetry-adapted simulation of solids. *Journal of the Chemical Society, Faraday Transactions*, **93**, 629 (1997)

(45) Z. Klika; H. Weissmannová; P. Capková; M. Pospíšil. The rhodamine B intercalation of montmorillonite. *Journal of Colloid and Interface Science*, **275**, 243 (2004)

(46) F. López Arbeloa; R. Chaudhuri; T. Arbeloa López; I. López Arbeloa. Aggregation of Rhodamine 3B Adsorbed in Wyoming Montmorillonite Aqueous Suspensions. *Journal of Colloid and Interface Science*, **246**, 281 (2002)

(47) V. Martínez Martínez; F. López Arbeloa; J. Bañuelos Prieto; T. Arbeloa López; I. López Arbeloa. Characterization of Rhodamine 6G Aggregates Intercalated in Solid Thin Films of Laponite Clay. 1. Absorption Spectroscopy. *The Journal of Physical Chemistry B*, **108**, 20030 (2004)

## 2. Experimental details and materials

Composite R6G/TiO<sub>2</sub> and R800/TiO<sub>2</sub> thin films were prepared by using porous TiO<sub>2</sub> thin films as host materials. For this purpose, transparent and amorphous TiO<sub>2</sub> were prepared by Glancing Angle Physical Vapor Deposition (GAPVD) at room temperature on quartz and silicon substrates. Evaporation was carried out in an electron bombardment evaporator by using TiO<sub>2</sub> pellets as target material. Stoichiometric thin films of TiO<sub>2</sub> were obtained by performing the evaporation in 10<sup>-4</sup> torrs of O<sub>2</sub>. The evaporation was carried out by placing the substrates at a glancing angle of 70° with respect to the evaporator source. This geometry produces films with a tilted columnar microstructure with a high porosity<sup>19-21</sup>. The films with a thickness around 400 nm were prepared by this method. In the present case the porosity of the films was estimated to be 35% of the total volume of the films, with a 70% of pores consisting of mesopores. A full account of the characteristics of these films can be found in a previous publication<sup>14</sup>.

The microstructure of the TiO<sub>2</sub> thin films deposited on a silicon wafer was examined by Field Emission Scanning Electron Microscopy (FESEM) in a Hitachi S5200 microscope. Cross sectional views were obtained by cleaving the silicon substrates.

UV-visible absorption spectra in transmission mode were recorded with a Perkin-Elmer Lambda 12 spectrometer for the thin films deposited on quartz plates. Although the absorbance is the typical magnitude used for presenting UV-vis absorption spectra of dyes in liquid solutions, we present here some spectra as the percentage of transmitted light. We have made this choice because this is the usual way of presenting these data when using optical thin films<sup>22</sup>.

1  
2  
3 A chloride salt of R6G and R800 dye molecules was used for the experiments. The salts  
4  
5 were supplied by ALDRICH and used without further purification. In solution, the  
6  
7 cationic R6G or R800 bear a positive charge, a feature that is essential for the  
8  
9 incorporation of the dye into the TiO<sub>2</sub> thin films.  
10  
11

12  
13 A 10<sup>-4</sup> M solutions of the dyes in water at controlled values of pH were used for  
14  
15 the infiltration experiments. The pH of the solution was controlled between 1.9 and 6.6  
16  
17 by adding giving amounts of HCl or NaOH. The TiO<sub>2</sub> films were immersed in one of  
18  
19 these solutions and maintained there for 10 min. The samples were then removed from  
20  
21 the solution and washed with water at the same pH than that of the dye solutions. In  
22  
23 general, the intensity of the colour of the films changed with the pH of the solution, a  
24  
25 feature that suggests the dependence between this parameter and the ability to incorporate  
26  
27 the dye molecules into the films.  
28  
29  
30  
31  
32

33 Figure 1 shows a series of UV-vis transmission spectra recorded for TiO<sub>2</sub> thin  
34  
35 films containing different concentrations of R6G and R800, as indicated in Table 1. The  
36  
37 spectra are characterized by the presence of a series of bands typical of the R6G dye  
38  
39 molecules (i.e., bands centred at ~520 nm) and R800 (i.e., bands centred at ~650 nm)<sup>14</sup>  
40  
41 superimposed on the typical oscillations due to interference phenomena between a  
42  
43 substrate and a transparent layer of different refraction index<sup>14</sup>. For the purposes of the  
44  
45 present work, the most important result is the dependence of the intensity of the features  
46  
47 attributed to the two dye molecules and the pH of the solution used for the preparation of  
48  
49 the films. Thus, it is observed that the intensity of the R6G features are strongly  
50  
51 dependent on the pH, increasing with this parameter. By contrast, R800 is little or no  
52  
53 sensitive to this parameter and the intensity of its spectral features remains almost  
54  
55  
56  
57  
58  
59  
60

constant for all the pHs. This different behaviour suggests that these two molecular cations interact differently with the surface of TiO<sub>2</sub> and that, particularly for the R800, the state of charge on the TiO<sub>2</sub> does not affect significantly the adsorption of this molecule.

3

Page 22: [2] Deleted

saidhg

3/27/2009 2:02:00 PM

Atom name	Force Field type	Charge	Atom name	Force Field type	Charge
<b>C1</b>	C_R	0,48	<b>O3</b>	O_2	-0.46
<b>C2</b>	C_R	-0.139	<b>C27</b>	C_3	0.346
<b>C3</b>	C_R	-0.287	<b>C28</b>	C_3	-0.25
<b>C4</b>	C_R	0.114	<b>H1</b>	H_	0.173
<b>C5</b>	C_R	0.287	<b>H2</b>	H_	0.231
<b>C6</b>	C_R	-0.438	<b>H3</b>	H_	0.238
<b>O1</b>	O_R	-0.385	<b>H4</b>	H_	0.17
<b>C7</b>	C_R	0.487	<b>H5</b>	H_HB	0.365
<b>C8</b>	C_R	-0.136	<b>H6</b>	H_	0.139
<b>C9</b>	C_R	0.08	<b>H7</b>	H_	0.15
<b>C10</b>	C_R	-0.46	<b>H8</b>	H_	0.155
<b>C11</b>	C_R	0.31	<b>H9</b>	H_	0.148
<b>C12</b>	C_R	0.106	<b>H10</b>	H_	0.089
<b>C13</b>	C_R	-0.285	<b>H11</b>	H_	0.123
<b>N1</b>	N_R	-0.534	<b>H12</b>	H_	0.083
<b>C14</b>	C_R	0.428	<b>H13</b>	H_	0.125
<b>C15</b>	C_R	-0.298	<b>H14</b>	H_	0.093
<b>C16</b>	C_R	-0.058	<b>H15</b>	H_	0.089
<b>C17</b>	C_R	-0.161	<b>H16</b>	H_	0.045
<b>C18</b>	C_R	-0.083	<b>H17</b>	H_	0.054
<b>C19</b>	C_R	-0.302	<b>H18</b>	H_	0.079
<b>C20</b>	C_3	-0.286	<b>H19</b>	H_	0.087
<b>C21</b>	C_3	-0.303	<b>H20</b>	H_HB	0.357
<b>C22</b>	C_3	0.166	<b>H21</b>	H_	0.063
<b>C23</b>	C_3	-0.232	<b>H22</b>	H_	0.041
<b>N2</b>	N_R	-0.521	<b>H23</b>	H_	0.033
<b>C24</b>	C_3	0.205	<b>H24</b>	H_	0.079
<b>C25</b>	C_3	-0.242	<b>H25</b>	H_	0.061

<b>C26</b>	C_2	0.784	<b>H26</b>	H_	0.088
<b>O2</b>	O_1	-0.532	<b>H27</b>	H_	-0.001
<b>O3</b>	O_2	-0.46	<b>H28</b>	H_	0.002
<b>C27</b>	C_3	0.346	<b>H29</b>	H_	0.071
<b>C28</b>	C_3	-0.25	<b>H30</b>	H_	0.084
<b>H1</b>	H_	0.173	<b>H31</b>	H_	0.085

**Table 3**

Atomic charges and DREIDING force field types of the atoms of rhodamine 6G shown in Figure 3a.

.....Page Break.....

Atom name	Force Field type	Charge	Atom name	Force Field type	Charge
<b>C1</b>	C_R	0.18	<b>H3</b>	H_	0.074
<b>C2</b>	C_R	0.057	<b>C24</b>	C_3	-0.008
<b>C3</b>	C_R	-0.365	<b>H4</b>	H_	0.078
<b>C4</b>	C_R	0.181	<b>C25</b>	C_3	0.046
<b>C5</b>	C_R	-0.061	<b>C26</b>	C_3	-0.161
<b>C6</b>	C_R	-0.058	<b>N3</b>	N_1	-0.417
<b>O1</b>	O_R	-0.183	<b>H5</b>	H_	0.059
<b>C7</b>	C_R	0.242	<b>H6</b>	H_	0.069
<b>C8</b>	C_R	0.033	<b>H7</b>	H_	0.094
<b>C9</b>	C_R	-0.064	<b>H8</b>	H_	0.055
<b>C10</b>	C_R	-0.137	<b>H9</b>	H_	0.054
<b>C11</b>	C_R	0.005	<b>H10</b>	H_	0.053
<b>C12</b>	C_R	0.14	<b>H11</b>	H_	0.029
<b>C13</b>	C_R	-0.344	<b>H12</b>	H_	0.038
<b>N1</b>	N_R	-0.002	<b>H13</b>	H_	0.09
<b>C14</b>	C_1	0.417	<b>H14</b>	H_	0.028
<b>C15</b>	C_3	-0.131	<b>H15</b>	H_	0.074
<b>C16</b>	C_3	-0.137	<b>H16</b>	H_	0.1
<b>C17</b>	C_3	-0.016	<b>H17</b>	H_	0.05
<b>C18</b>	C_3	-0.06	<b>H18</b>	H_	0.058
<b>N2</b>	N_R	0.085	<b>H19</b>	H_	0.027
<b>C19</b>	C_3	-0.143	<b>H20</b>	H_	0.059
<b>C20</b>	C_3	0.016	<b>H21</b>	H_	0.042
<b>H1</b>	H_	0.211	<b>H22</b>	H_	0.098
<b>C21</b>	C_3	-0.017	<b>H23</b>	H_	0.048
<b>C22</b>	C_3	0.018	<b>H24</b>	H_	0.043
<b>H2</b>	H_	0.209	<b>H25</b>	H_	0.075
<b>C23</b>	C_3	-0.011	<b>H26</b>	H_	0.082

**Table 4**

Atomic charges and DREIDING force field types of the atoms of rhodamine 800 shown in Figure 3b.

.....Page Break.....

For Peer Review Only